Laboratori Nazionali di Frascati

LNF-70/64

P. Picozza, C. Schaerf, R. Scrimaglio, G. Goggi, A. Piazzoli and D. Scannicchio : AN EXPERIMENTAL INVESTIGATION OF MESON EFFECTS IN HIGH-ENERGY PHOTODISINTEGRATION OF LIGHT NUCLEI

Estratto da : Nuclear Phys. A157, 190 (1970)

2.I

Nuclear Physics A157 (1970) 190—208;

AN EXPERIMENTAL INVESTIGATION OF MESON EFFECTS IN HIGH-ENERGY PHOTODISINTEGRATION OF LIGHT NUCLEI

P. PICOZZA, C. SCHAERF and R. SCRIMAGLIO

Laboratori Nazionali di Frascati del CNEN, Frascati, Italy

and

G. GOGGI, A. PIAZZOLI and D. SCANNICCHIO

Istituto di Fisica dell'Università di Pavia and Istituto Nazionale di Fisica Nucleare, Gruppo Pavia, Pavia, Italy

Received 3 July 1970

Abstract: The ^{3}He(γ, p)d and ^{4}He(γ, p)t differential cross sections at 90° in the c.m.s. have been measured in the γ-ray energy region 200–500 MeV using a liquid helium target and spark chamber technique. The ^{4}He photodisintegration shows a resonant behaviour in the energy interval 240–330 MeV, not observed in the ^{3}He process.

Such different behaviour can be tentatively interpreted, in analogy with deuteron photodisintegration, on the basis of a pion photoproduction and the re-absorption model.

E NUCLEAR REACTIONS ^{3}He(γ, p), ^{4}He(γ, p), E = 200–500 MeV; measured σ(E). Natural target.

1. Introduction

The photodisintegration of light nuclei constitutes a relevant tool for the study of their dynamical properties. The ^{3}He and ^{4}He nuclei are the first stable nuclei with more than two nucleons and therefore a necessary starting point for a systematic study of nuclear forces and nuclear structure in the few-body systems.

In the last years many experiments [1–8]) and theoretical calculations [9,10]) have been performed on the two- and three-body photodisintegration of ^{3}He in the energy range between threshold and 150 MeV. In particular for two-body photodisintegration a good interpretation of the experimental data can be obtained up to γ-ray energies of about 60 MeV. For higher energies estimates have been made taking into account the electromagnetic interaction in the form $A \cdot p$ or $E \cdot r$ to all orders of multipolar expansion and using different ground state wave functions for ^{3}He [ref. [10])].

No attempts have been made to take rigorously into account the meson exchange currents and relativistic corrections. The interaction with the nucleon current in the form $A \cdot p$ gives theoretical results much lower than the experimental data for all reasonable choices of the nuclear wave functions. It now seems clear that this dis-

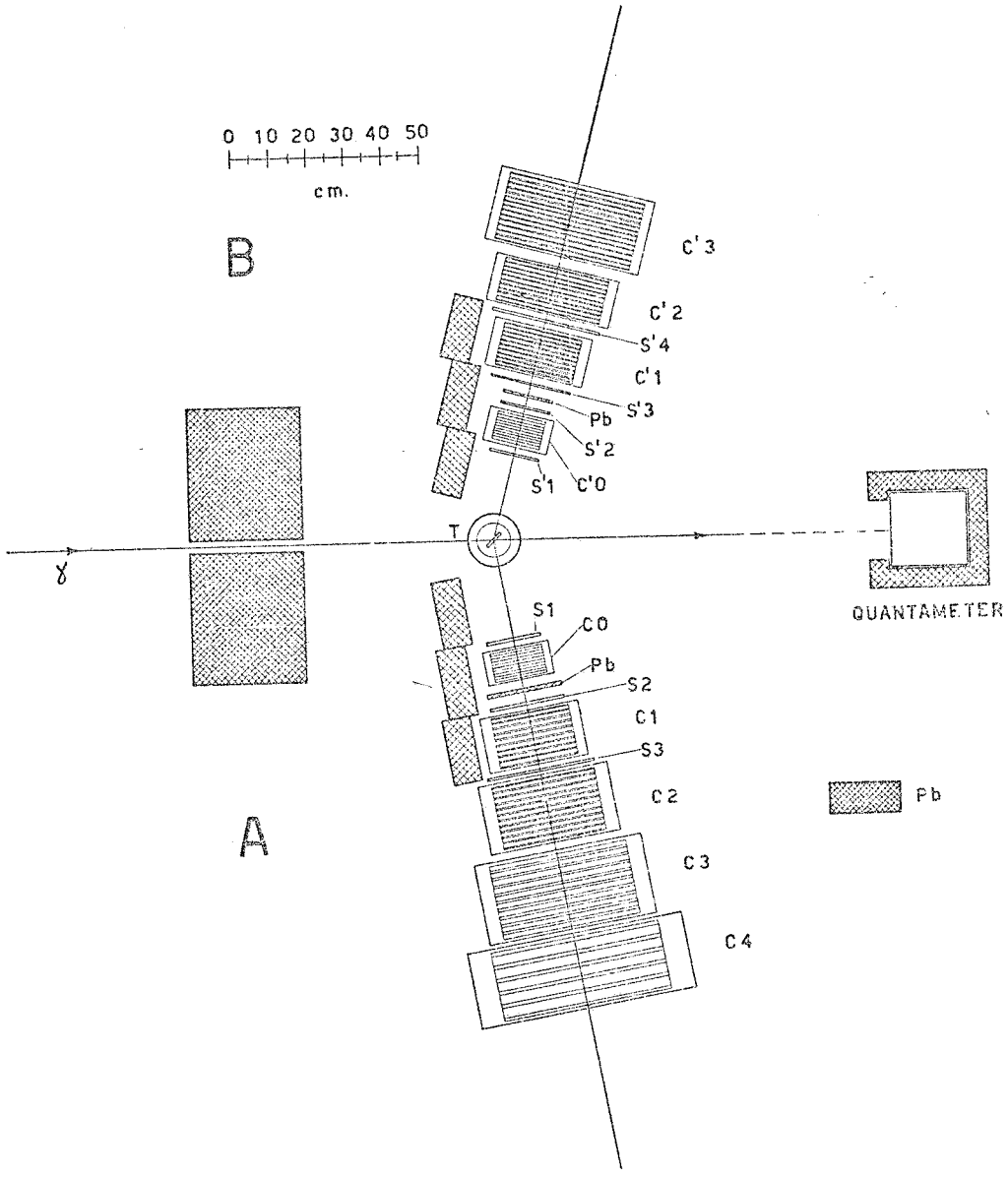

Fig. 1. Experimental set-up: T, liquid He target; S_1, S_2, S_3, S'_1, S'_2, S'_3, S'_4, scintillation counters; C_1, C_2, C_3, C_4, C'_1, C'_2, C'_3, spark chambers for range measurements; C_0, C'_0, spark chambers for angle measurements.

crepancy cannot be overcome by just choosing more refined wave functions for the three-nucleon systems or introducing a variety of final state interactions.

From the experimental point of view a similar situation exists for the (γ, p) photo disintegration reaction on ^{4}He [refs. [11–14])] which is sufficiently understood theoretically only at low energies [refs. [15–17])].

In this paper we present our final results [18,19]) on the differential cross sections for the two-body photodisintegration of ^{3}He and ^{4}He at 90° in the c.m.s. in the energy interval 200–500 MeV, where the possible contributions of meson currents and new reaction mechanisms are expected to be more evident.

Some aspects of these results are discussed together with those on the photodisintegration of the deuteron from various authors [20,21]). In the following we will fix our attention on the reactions

$$\gamma + d \rightarrow p + n, \qquad (1$$

$$\gamma + {}^3\mathrm{He} \rightarrow p + d, \qquad (2$$

$$\gamma + {}^4\mathrm{He} \rightarrow p + t \qquad (3$$

and discuss their properties above pion threshold.

The experimental apparatus is described in the next section. Sects. 3 and 4 refer to the evaluation of measurement errors and to the selection criteria for reactions (2) and (3). Sect. 5 describes the data corrections and in sect. 6 the experimental results are discussed. In the appendix some considerations about the convenience of using these reactions for time reversal tests are given.

2. Experimental arrangement

A plane view of the experimental arrangement, as used to measure reaction (2), is shown in fig. 1.

An 800 MeV bremsstrahlung beam from the Frascati electrosynchrotron was collimated and cleared by a sweeping magnet before entering a long vacuum pipe followed by the liquid ^{3}He target.

The experimental area was shielded from the synchrotron by concrete and lead walls. Downstream the target the beam was monitored by a Wilson-type quantameter.

The liquid ^{3}He target is extensively described in ref. [22]). Its essential part is a lens-shaped cell, with a maximum thickness of 17.5 mm, consisting of two nickel foils 0.03 mm thick welded to a rectangular nickel frame 40×80 mm^2.

The cell was oriented at 45° with respect to the beam axis. The temperature of the liquid ^{3}He was 2.5 °K, corresponding to a density of 74.5 mg/cm^3 and was regularly controlled throughout the runs by monitoring the pressure in the gaseous ^{3}He reservoir. The spot of the collimated γ-ray beam at the cell was 20 mm in diameter. The total thickness of material (liquid ^{3}He, nickel foils, mylar windows) traversed by particles before entering the detection apparatus corresponded to 170 mg/cm^2 of Al.

As shown in fig. 1 the detection apparatus consisted of two asymmetric telescopes labelled A and B of plastic scintillators and optical spark chambers. In order to observe reactions (2) and (3) around $\theta_{c.m.s.} = 90°$ in the γ-energy range 200–500 MeV the channels A and B were centered in the laboratory at angles of about 80° and 75° respectively.

Telescope A consisted of 3 plastic scintillators 6 mm thick and 5 spark chambers. The spark chambers were of the conventional type with 6 mm gaps, square aluminium plates and open circuit gas circulation. The first one, with a constant plate thickness of 25 μm, was used for a measurement of the angle of the particles. The remaining 4 spark chambers measured the ranges of the detected particles; in order to maintain a practically constant percentage error on the determination of momentum for the reaction products the thickness of the Al plates was increased from 2 mm in the second

TABLE 1

Geometrical and kinematical characteristics of the apparatus

Target nucleus	θ_{lab}		p (MeV/c)		$\theta_{c.m.}$	E_γ (MeV)
	channel A	channel B	channel A	channel B		
^{3}He (reaction (2))	71.5°–85°	63.6–79.7°	497–920	497– 900	75°–105°	185–560
^{4}He (reaction (3))	71.5°–85°	63.6–79.7°	460–927	514–1170	74°– 99°	190–580

to 25 mm in the fifth spark chamber. The total number of gaps in the range telescope was 36 with a total thickness of 321 mm. The channel B, similar to the previous one, consisted of 4 plastic scintillators and a set of 4 chambers, the first, used for a measurement of the angle, being identical to the first one in channel A. The remaining three chambers were used for range measurements and their plate thickness increased from 0.3 to 6 mm, with 36 gaps and a total thickness of 69.2 mm.

The first three plastic scintillators were 2 mm thick and the fourth was 6 mm thick. The solid angle subtended by the apparatus was 0.055 sr. The signals from the seven scintillators were elaborated through a fast electronic logic developed by the LNF Electronic Group. All coincidences were monitored during the runs for stability controls. For every triggering signal, defined as a seven-fold coincidence, a stereoscopic photograph was taken for each channel. In order to perform a measurement of reaction (3) with results directly comparable to those concerning reaction (2) minor modifications were introduced in the experimental apparatus. In channel A a thicker lead absorber (3 mm thick) was placed between the "angle" and "range" chambers, whereas in channel B the counter S4 was eliminated thus lowering the triggering signal to a six-fold coincidence.

The target was filled with ^{4}He at a temperature of 2.97 °K corresponding to a density of 142 mg/cm^3.

In reaction (2), the range and angle were measured in channel A for the proton and in channel B for the deuteron. Similarly in reaction (3) protons were detected in channel A whereas tritons were detected in channel B.

As will be discussed in more detail in sect. 4, there is no ambiguity in interchanging the particles with respect to the channels. Table 1 lists the main geometrical and kinematical characteristics of the apparatus in the two mentioned measurements.

3. Evaluation of measurement errors

The main sources of experimental errors considered were the measurements of the angles and ranges of the reaction products and the empty cell background. The absolute accuracy of the quantameter was of the order of 5 % and the uncertainty in the density of both liquids (^{3}He and ^{4}He) was 0.7 %.

Two kind of errors gave the main contributions to the uncertainty in the angle measurement: multiple Coulomb scattering in the material traversed by the particles before detection and spatial jitter of the sparks in the angle chambers.

Total angular errors for the different particles detected were:

$$\sigma_{\text{protons}} \approx 3^\circ; \qquad \sigma_{\text{deuterons}} \approx 3^\circ; \qquad \sigma_{\text{tritons}} \approx 5^\circ.$$

The main uncertainty in the momentum measurements arose from the discrete resolution of the system of range spark chambers due to the plates' thickness. As a design choice the progression of thicknesses was such that

$$\left.\frac{\Delta p}{p}\right|_{\text{protons}} = 2.7\,\%; \qquad \left.\frac{\Delta p}{p}\right|_{\text{deuterons}} = 2.1\,\%; \qquad \left.\frac{\Delta p}{p}\right|_{\text{tritons}} = 2.5\,\%.$$

The empty cell background was independently measured and the correlated events reconstructed with the same procedure used for the events produced in the full target. The corresponding results, properly normalized, are shown for a direct comparison in each relevant distribution concerning the accepted events. This background was then properly subtracted from the raw data.

4. Selection criteria of the events

With the apparatus described in the previous sections operating in the seven-fold coincidence mode, reaction (2) can be detected and measured only for a proton entering channel A and a deuteron entering channel B. In fact the kinematics of reaction (2) is such that for the reversed reaction, i.e. a p entering channel B and a d entering channel A, the following is true: (i) the energy of the deuteron is not sufficient to give a signal in counter S3, or (ii) the range of the proton in Al is greater than the total thickness of channel B.

The rejection of these events is trivial: the electronic requirement for a trigger is not satisfied in case (i); in case (ii) the photographs indicate immediately that the particle in channel B traversed the last plate of the range telescope.

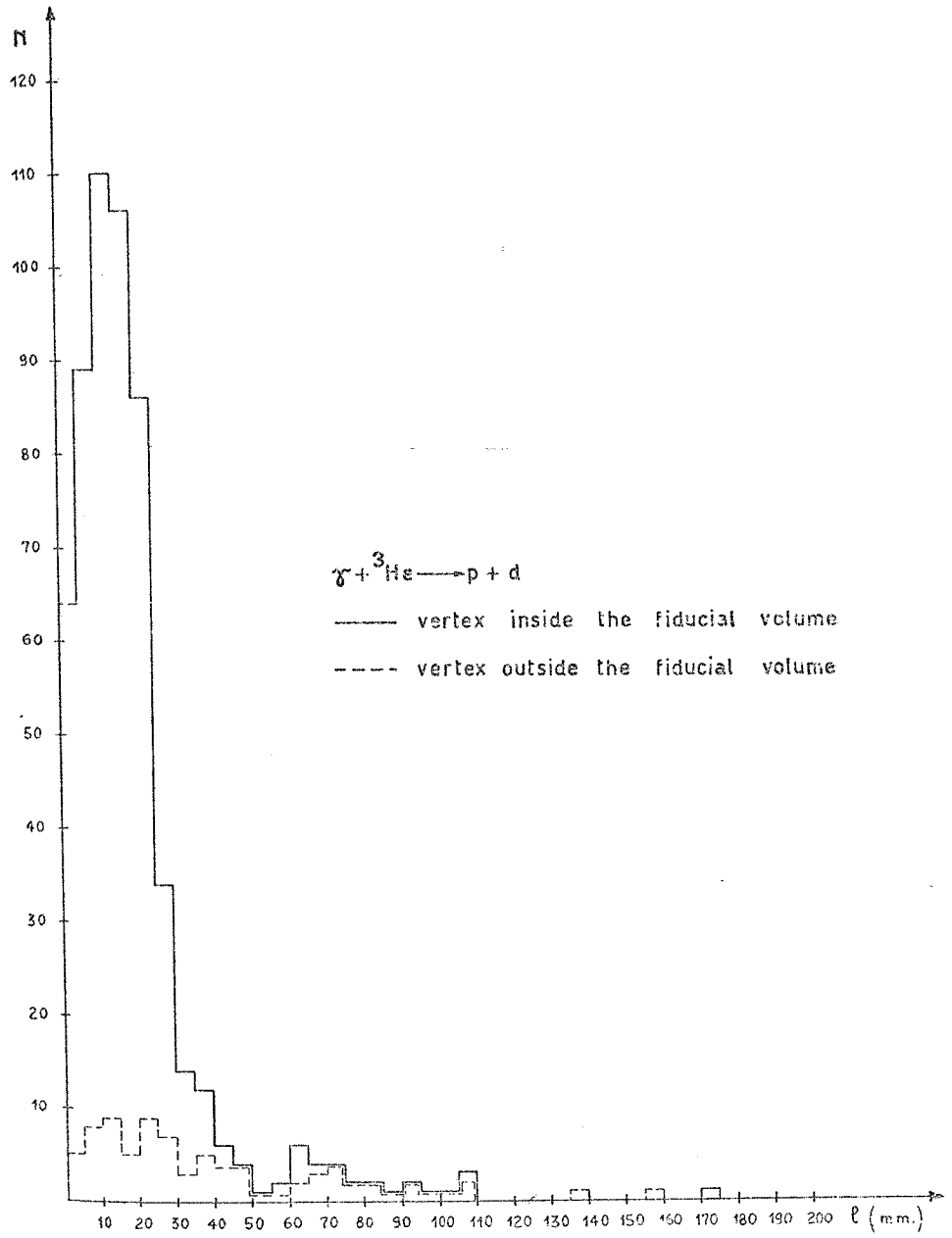

Fig. 2. Sample distribution of the least distance segment between two measured tracks for reaction (3). The dashed line represents the distribution for events with the vertex outside the fiducial volume.

For reaction (3), operating in the six-fold coincidence mode, a similar situation is given.

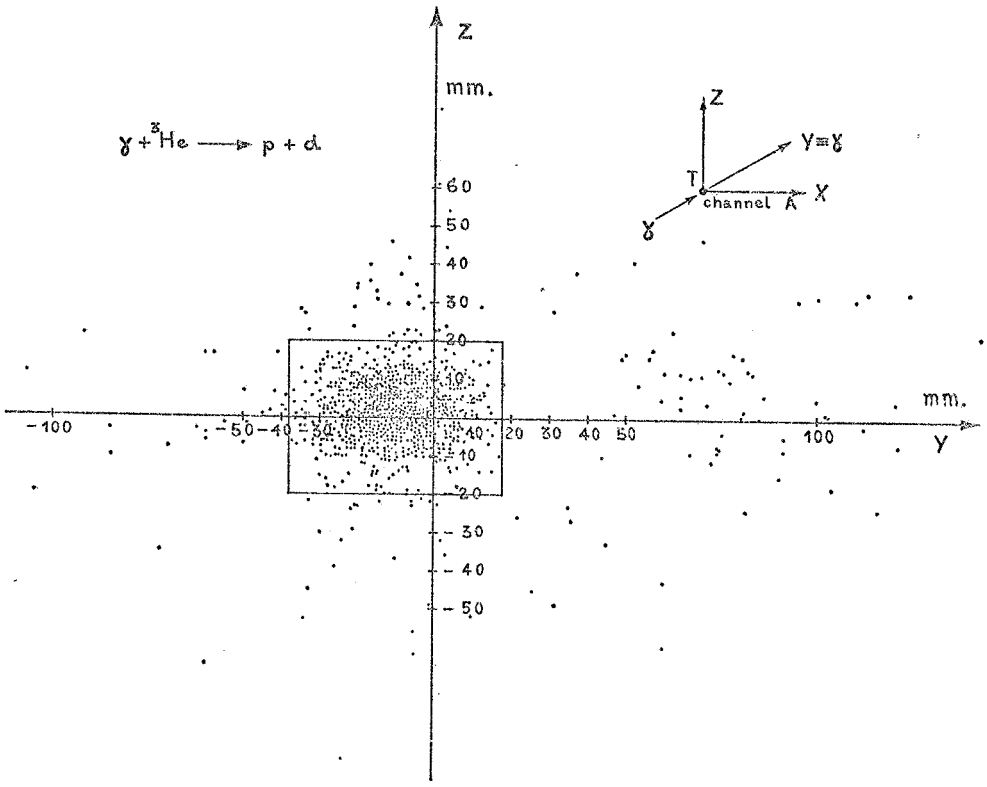

Fig. 3. Sample distribution in the plane y (γ-ray axis) z (vertical axis) of the vertices for reaction (2). The fiducial limits are indicated.

For both reactions the events were spatially reconstructed and the position of the geometrical vertex computed. This is defined as the mean point in the least distance segment of the two measured tracks. The distribution of lengths of this segment is shown in fig. 2. Events with the vertex lying outside a fiducial volume were rejected. In fig. 3 a sample of the space distribution of the vertices is plotted; the fiducial limits, compatible with the true target dimensions, are indicated.

A further selection was made on the coplanarity of the measured tracks. Events satisfying all these requirements were kinematically reconstructed with a linearized two-parameter fit.

The resulting χ^2 distributions gave rise to the last selection criterium. In this way a total of 3033 events were selected for reaction (2) and 1958 for reaction (3).

5. Data corrections

The foregoing analysis gives the distributions of the selected events as a function of the γ-ray energy, a sample of which is shown in figs. 4 and 5.

The empty cell background and the full target counts are presented. The events have been selected with the criteria indicated in the previous section.

These distributions, besides background subtraction and normalization to the bremsstrahlung spectrum, have to be weighted by an energy-dependent efficiency factor, but even before any further elaboration a comparison of the distributions of the raw data shows different energy behaviours in the first half of the measured inter-

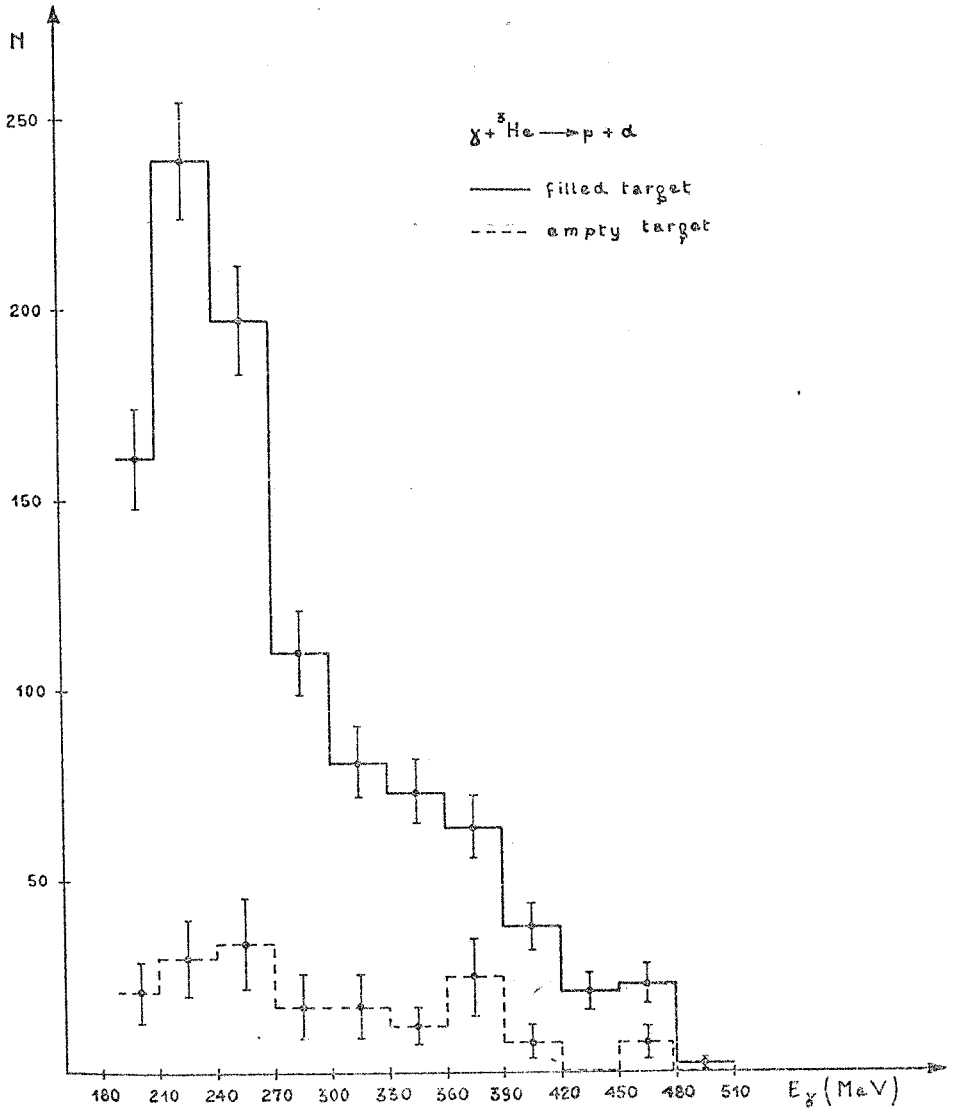

Fig. 4. Sample distribution of the events for the reaction $\gamma + {}^3\mathrm{He} \rightarrow \mathrm{p} + \mathrm{d}$ satisfying all selection criteria. The dashed line represents the distribution of empty target events.

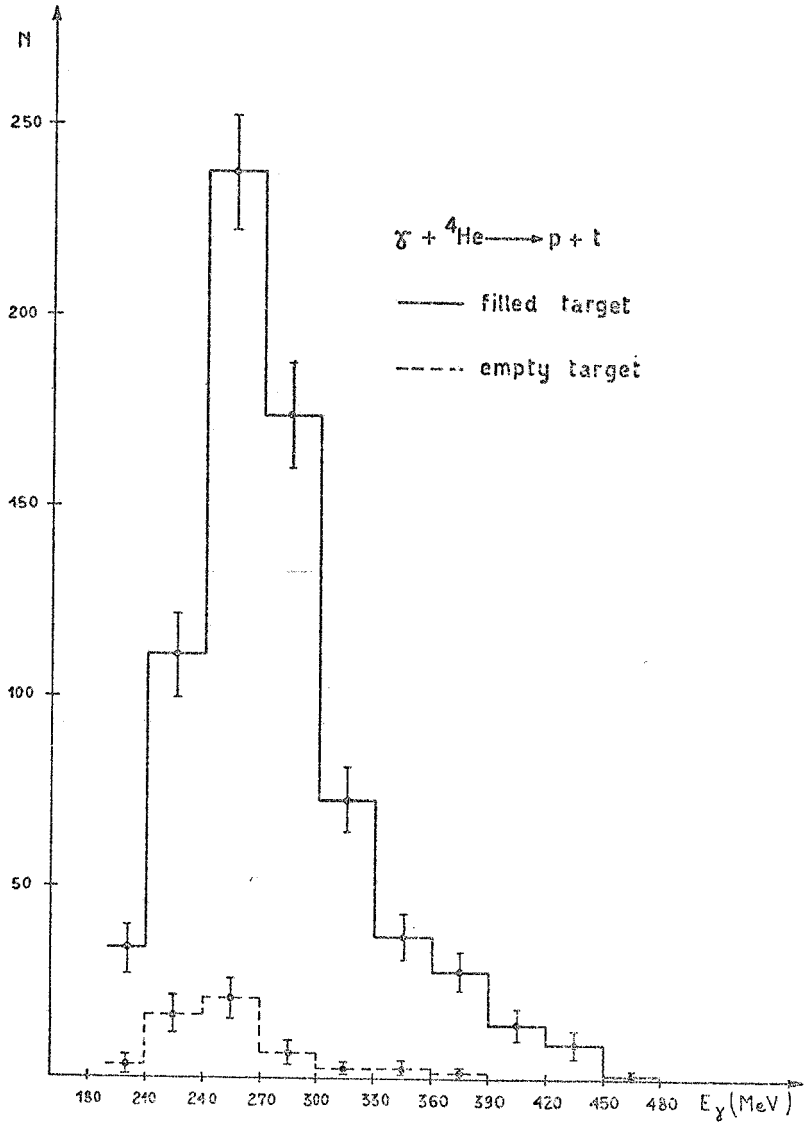

Fig. 5. Sample distribution of the events for the reaction $\gamma + {}^4He \rightarrow p + t$ satisfying all selection criteria. The dashed line represents the distribution of empty target events.

val. The detection efficiency of the experimental apparatus versus γ-ray energy is mainly determined by three different factors.

(i) the geometrical layout, which affects the shape of the kinematical phase space available to the reaction;

(ii) the inelastic nuclear scattering of the particles in the aluminium plates, which affects the measured range of the secondaries;

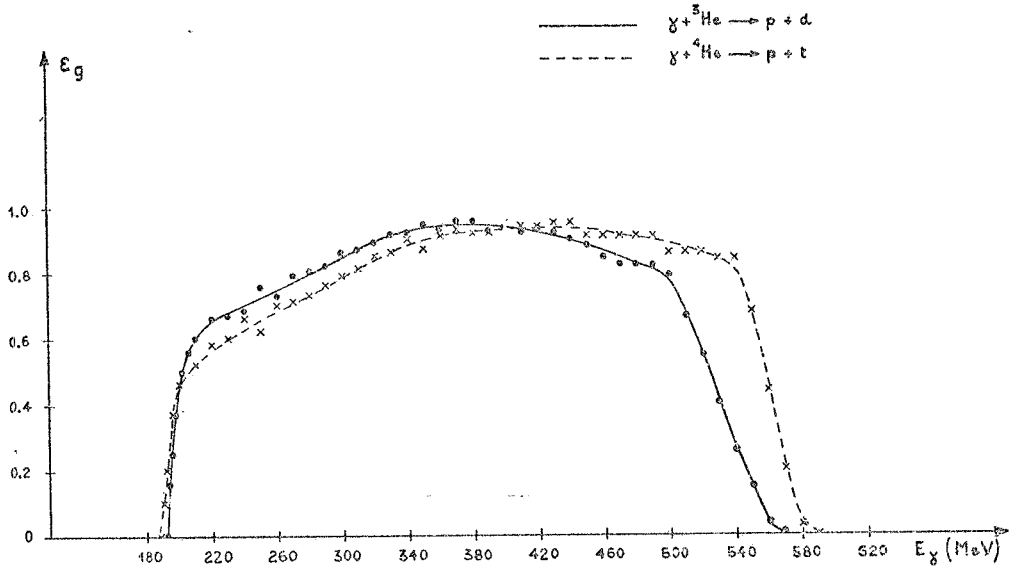

Fig. 6. Geometrical-kinematical efficiencies of the apparatus for the reactions $\gamma+{}^3\mathrm{He} \rightarrow \mathrm{p}+\mathrm{d}$ (straight line) and $\gamma+{}^4\mathrm{He} \rightarrow \mathrm{p}+\mathrm{t}$ (dashed line).

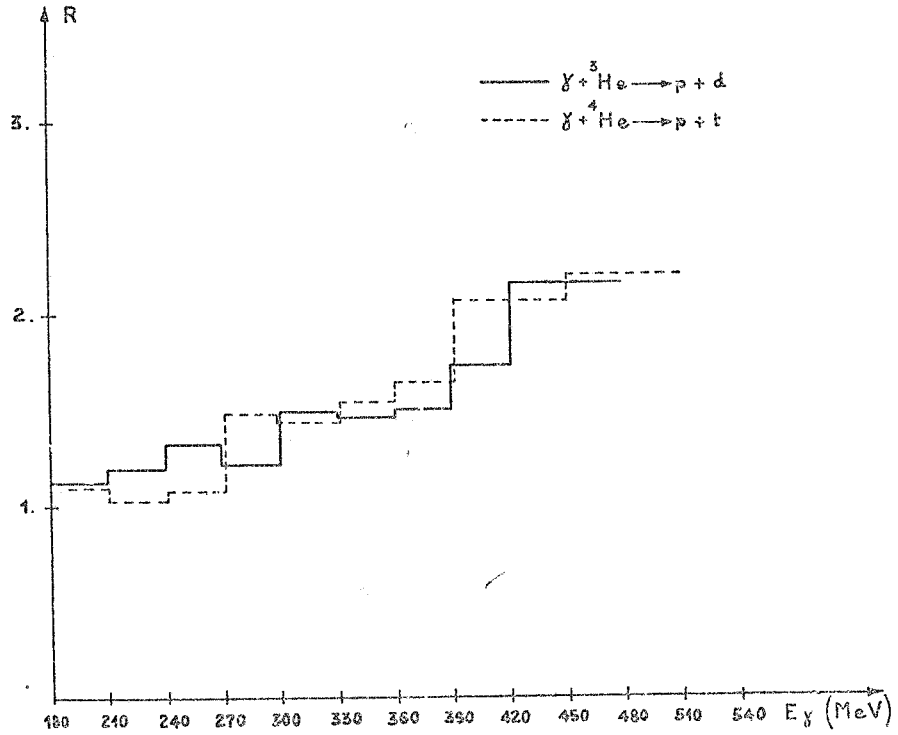

Fig. 7. Ratio R between events corrected by nuclear scattering and single gap efficiencies and uncorrected events for the reactions $\gamma+{}^3\mathrm{He} \rightarrow \mathrm{p}+\mathrm{d}$ (straight line) and $\gamma+{}^4\mathrm{He} \rightarrow \mathrm{p}+\mathrm{t}$ (dashed line).

(iii) the single-gap efficiency of the range chambers in both telescopes, which gives a similar effect.

The geometrical-kinematical efficiencies for reactions (2) and (3) were evaluated by means of a Monte Carlo calculation. The results of the calculations are shown in fig. 6 where the efficiencies for both reaction (2) and (3) are separately plotted. A special computer run was performed to analyze in greater detail the fast rising regions

TABLE 2

$\gamma + {}^3\mathrm{He} \rightarrow \mathrm{p} + \mathrm{d}$

E_γ (MeV)	$\left.\frac{\mathrm{d}\sigma}{\mathrm{d}\Omega}\right\|_{90°\ \mathrm{c.m.s.}}$ $(10^{-32}\ \mathrm{cm}^2)$
180–210	89.0±6.1
210–240	47.6±1.7
240–270	37.4±1.5
270–300	29.6±1.6
300–330	23.0±1.9
330–360	17.2±1.4
360–390	12.8±1.2
390–420	15.1±1.8
420–450	6.8±1.1
450–480	9.6±1.8
480–510	3.1±1.1
510–540	1.8±1.1
540–570	2.9±2.0

TABLE 3

$\gamma + {}^4\mathrm{He} \rightarrow \mathrm{p} + \mathrm{t}$

E_γ (MeV)	$\left.\frac{\mathrm{d}\sigma}{\mathrm{d}\Omega}\right\|_{90°\ \mathrm{c.m.s.}}$ $(10^{-32}\ \mathrm{cm}^2)$
195–210	20.1±2.0
210–240	18.2±1.1
240–270	33.8±1.6
270–300	46.0±2.1
300–330	19.9±1.5
330–360	13.7±1.2
360–390	8.8±1.0
390–450	5.2±0.7
450–510	0.3±0.2

above detection thresholds. As coplanarity is required by both reactions, the efficiency connected with the finite $\Delta\varphi$ acceptance of the apparatus was evaluated in an analogous way.

Scattering efficiency: the spread in γ-ray energy reconstruction and the related efficiency due to the inelastic nuclear scattering in the range chamber have been evaluated by means of a Monte Carlo calculation on the basis of the mean free paths

for inelastic scattering in aluminium as given in ref. [23]). A matrix technique of correction coefficients, which included correlation terms among different energy channels, was used in the raw data reduction [24]).

Gap efficiency: in the same way the small correction due to the single gap efficiency was evaluated on the basis of the gap efficiencies measured on different samples of photograms.

The combined effect of the last two corrections, both computed without considering the geometrical-kinematical efficiency of the apparatus, is given in fig. 7 for reac-

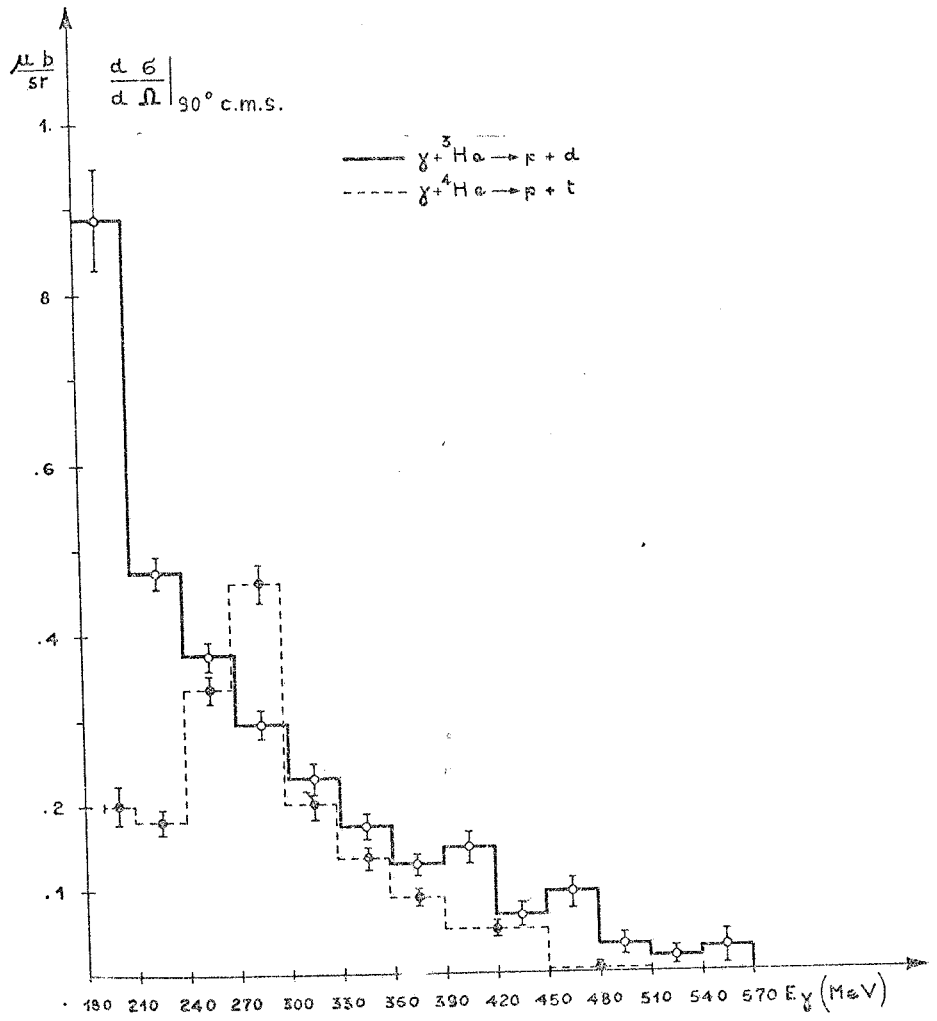

Fig. 8. Experimental differential cross sections at 90° in the c.m.s. for the reactions $\gamma+{}^3\mathrm{He} \rightarrow \mathrm{p}+\mathrm{d}$ (straight line) (○) and $\gamma+{}^4\mathrm{He} \rightarrow \mathrm{p}+\mathrm{t}$ (dashed line) (●).

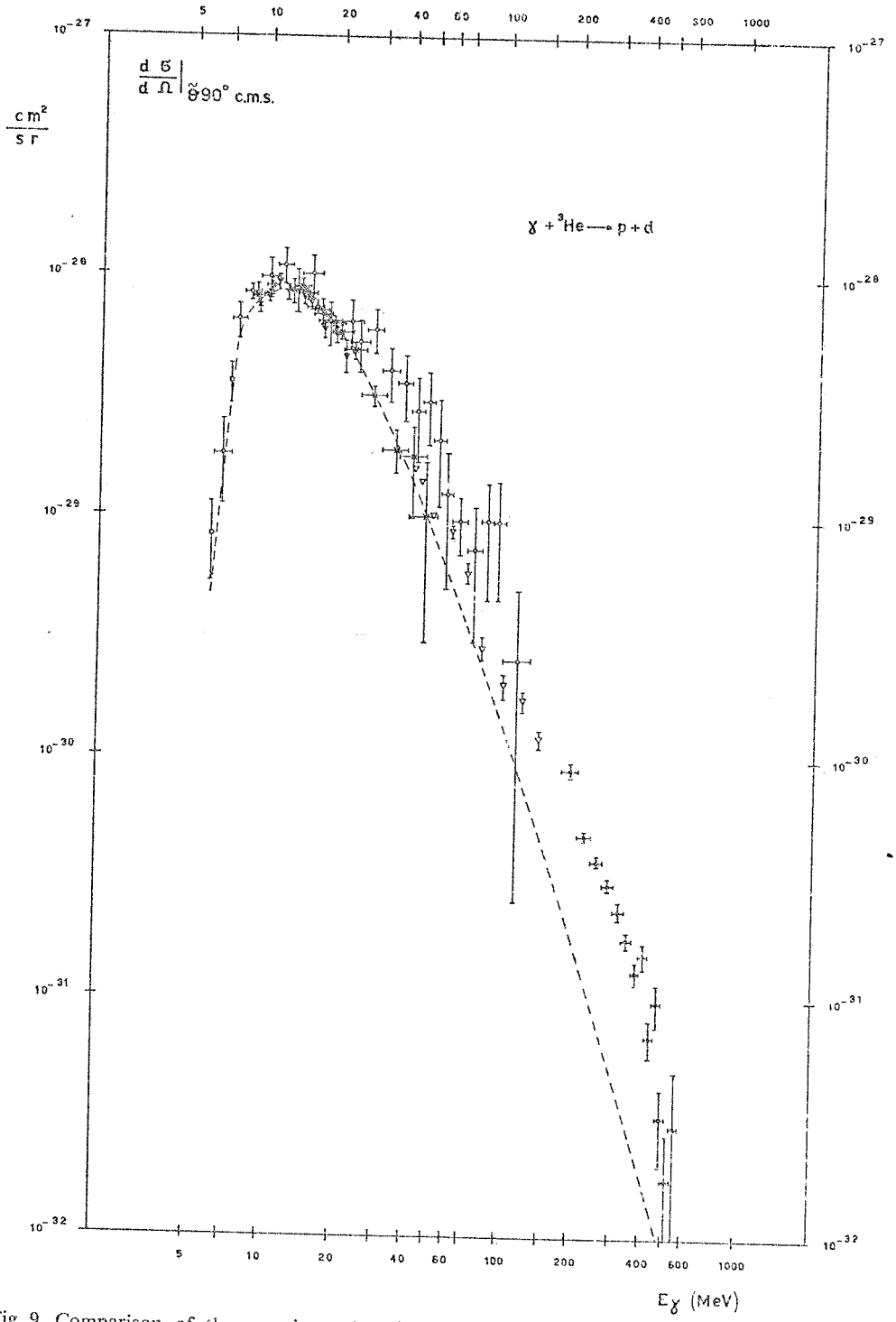

Fig. 9. Comparison of the experimental 90° c.m.s. differential cross section for the reaction $\gamma + {}^3\mathrm{He} \rightarrow \mathrm{p} + \mathrm{d}$. Assuming a $\sin^2 \tilde{\theta}$ angular distribution in the whole energy range, the data by Fetisov *et al.* and Bösh *et al.* have been multiplied by $\frac{3}{8}\pi$ to compare them with the other data. The dashed curve is the Gunn and Irving theoretical calculation with $\mu^{-1} = 2.6$ fm. (○) Fetisov *et al.* [6]) $\times \frac{3}{8}\pi$; (▽) Berman *et al.* [1]); (▨) Bösh *et al.* [5]) $\times \frac{3}{8}\pi$; (×) Stewart *et al.* [4]); (◉) this experiment; (▽) O'Fallon *et al.* [7]); (- - -) Gunn and Irving [9]) $1/\mu = 2.6$ fm.

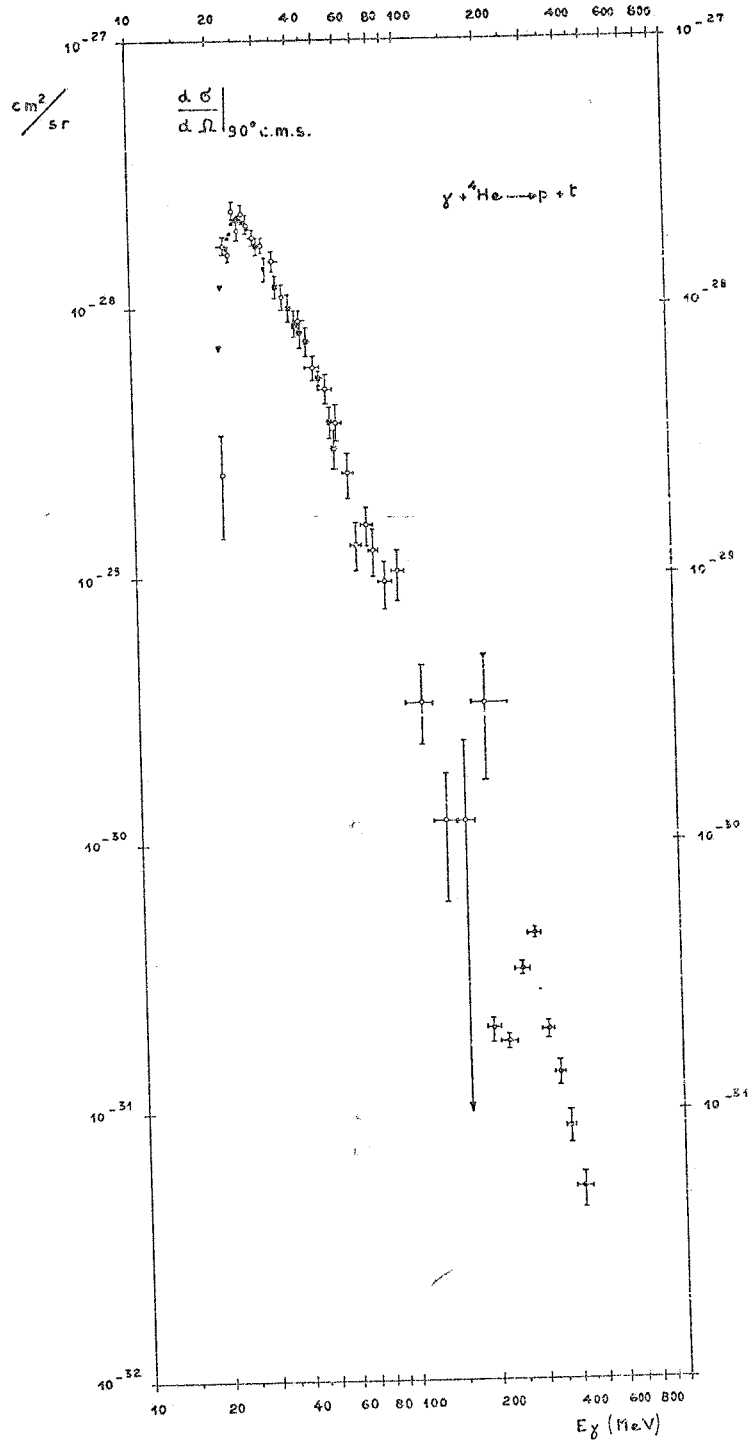

Fig. 10. Comparison of the experimental 90° c.m.s. differential cross section for the reaction $\gamma + {}^4\mathrm{He} \rightarrow \mathrm{p} + \mathrm{t}$. Assuming a $\sin^2\tilde{\theta}$ angular distribution in the whole energy range, the data by Gorbunov [11] (○); Clerc *et al.* [12] (×); Gemmell *et al.* [13] (△), have been multiplied by $\frac{8}{3}\pi$ to compare them with our data (◉); Perry *et al.* [14] (▽).

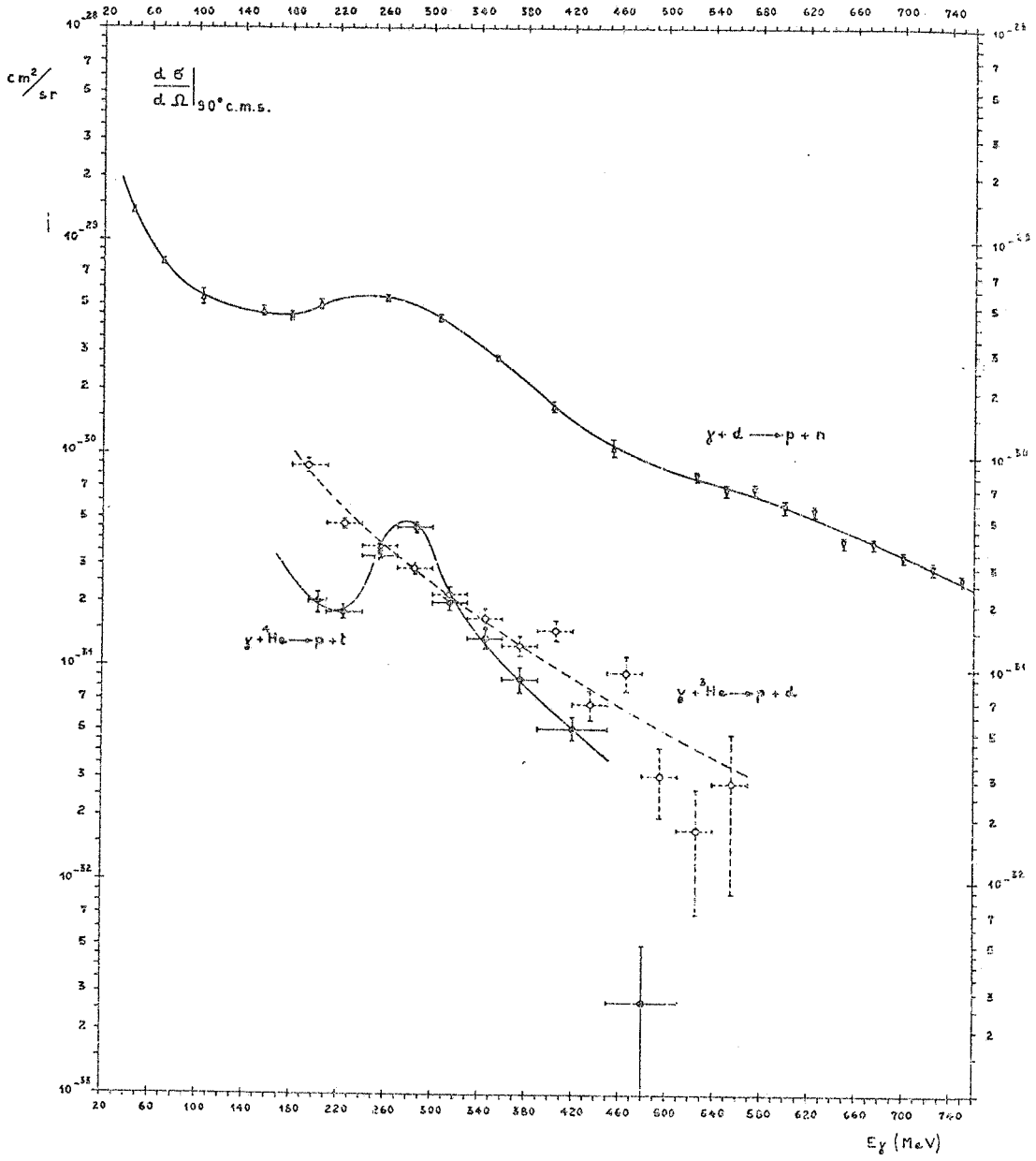

Fig. 11. Comparison of the experimental 90° c.m.s. differential photodisintegration cross sections in two bodies for d, ^{3}He, ^{4}He. (○) $\gamma + {}^3\mathrm{He} \rightarrow \mathrm{p} + \mathrm{d}$ (this experiment;) (●) $\gamma + {}^4\mathrm{He} \rightarrow \mathrm{p} + \mathrm{t}$ (this experiment); $\gamma + \mathrm{d} \rightarrow \mathrm{p} + \mathrm{n}$ (△) Keck *et al.* [20]) and (▽) Ching *et al.* [21]).

tions (2) and (3). It follows that the effects of all the quoted corrections on the data of reactions (2) and (3) are similar and do not introduce any anomalous modification in the shape of the energy distributions.

6. Results and discussion

Our results are shown in tables 2 and 3 and in fig. 8, where the differential cross sections for reaction (2) $\gamma+{}^3\mathrm{He} \rightarrow \mathrm{p}+\mathrm{d}$ and (3) $\gamma+{}^4\mathrm{He} \rightarrow \mathrm{p}+\mathrm{t}$ at 90° c.m.s. are both presented with statistical errors only. In fig. 9 the general behaviour of the lower energy experimental data on reaction (2) appears consistent with our results, in

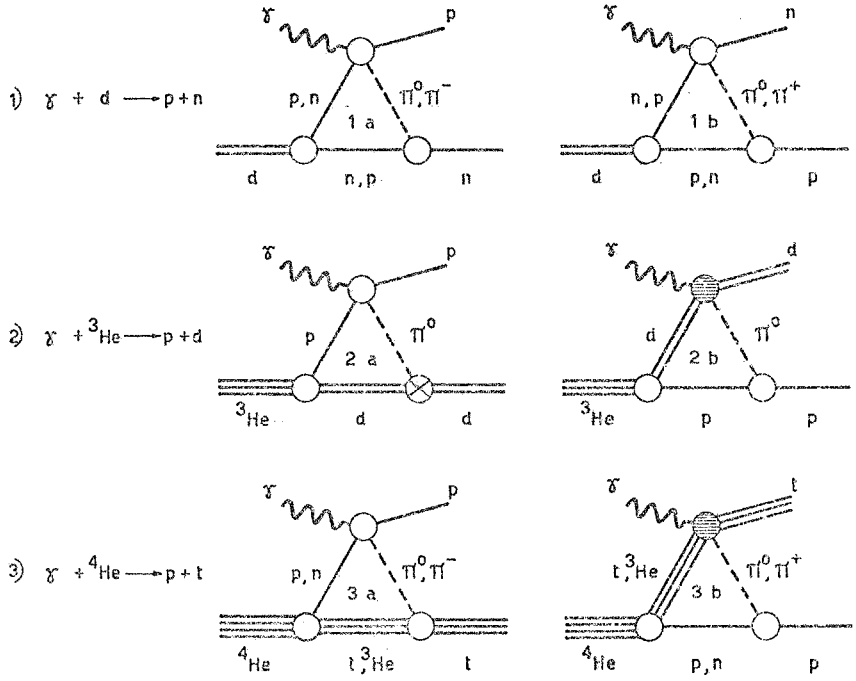

Fig. 12. Relevant diagrams for a possible resonant contribution in the reactions indicated. The crossed vertex in diagram 2a) is forbidden by isospin conservation and the dashed vertices in diagrams 1b) and 3b) are depressed and should not give a valuable resonant contribution.

particular with the measurements by O'Fallon *et al.* [7]) near the pion photoproduction threshold. Also for reaction (3) fig. 10 indicates a general consistency of our data with other experiments.

The most relevant feature of our measurements is the different behaviour of reactions (2) and (3) in the region of the (3, 3) pion-nucleon resonance. In fact fig. 11 shows a clear resonant behaviour both for reaction (3) and (1) $\gamma+\mathrm{d} \rightarrow \mathrm{p}+\mathrm{n}$, while no enhancement is observed for reaction (2). A phenomenological approach to these

features can be given on the basis of the model originally proposed by Austern [25]) and Wilson [26]) to understand the deuteron photodisintegration data taking into account the pion photoproduction and reabsorption. In fig. 12 we have indicated the diagrams relevant for a possible resonant contribution to these reactions. It is immediately clear from this figure that diagram 2a) is forbidden by isospin conservation in the vertex π^0d. On the other hand it is experimentally known [27]) that the coherent π^0 photoproduction on deuterium in the region of the (3, 3) resonance is depressed with respect to the photoproduction in hydrogen by the multiple pion nuclear scattering. This effect, which seems to be generalized to all light nuclei, reduces the probability of a resonant contribution of diagrams 2b) and 3b).

According to these simple considerations we can conclude that there should not be an appreciable resonant contribution for reaction (2) and that the contribution of the resonant amplitude to reaction (3) should be in absolute value much lower than to reaction (1).

It is a pleasure to thank Prof. A. Gigli for his constant support and encouragement. The cooperation of the machine staff and of the cryogenic group of the Laboratori Nazionali di Frascati is gratefully acknowledged.

Appendix

The arguments of sect. 6 can be used to investigate the possibilities to test time-reversal violation in the electromagnetic interactions of the hadrons.

We remark that reactions (2) and (3) are experimentally the most convenient for such research.

The hypothesis that the electromagnetic interactions of the hadrons are not invariant under time-reversal has been discussed by various authors [28,29]). A particular model has been introduced by Barshay [30]) to calculate the possible effect of this hypothesis in the inverse reactions:

$$\gamma + \mathrm{d} \leftrightarrows \mathrm{n} + \mathrm{p}. \tag{A.1}$$

This model introduces a failure of time-reversal invariance in the vertex

$$\gamma + \mathrm{N} \leftrightarrows \mathrm{N}^*, \tag{A.2}$$

where N indicates a nucleon and N* an isobar ($T = \frac{3}{2}$, $J = \frac{3}{2}$). This violation is in the form of a phase shift in the vertex representation which changes sign under time reversal.

Various experiments [31,32]) have been made to test this model.

Comparisons have been made of reactions (A.1) and the reactions

$$\gamma + {}^3\mathrm{He} \leftrightarrows \mathrm{p} + \mathrm{d}. \tag{A.3}$$

Only recently some tentative evidence has been claimed by a Princeton group [33]) in reactions (A.1).

However this study is made difficult by the problem of producing and monitoring a high-energy neutron beam. Reactions (A.3) appear easier at first sight but the results of our experiments suggest that no appreciable effect should be found there according to the Barshay model. In fact to have an effect there should have a significant contribution to the matrix element from the $NN^*\gamma$ vertex. This should show up as a bump in the cross section at a c.m. energy comparable with that of the first pion-nucleon resonance. As shown, no such bump is apparent in our ^{3}He data.

However there is a clear evidence of a resonant behaviour in the cross section for the photodisintegration of ^{4}He. Therefore we suggest that further search for a violation of time-reversal invariance should be made on the deuteron or ^{4}He. In particular the study of reactions

$$\gamma + {}^4\mathrm{He} \leftrightarrows \mathrm{p} + \mathrm{t}$$

appears very promising. In fact here a more pronounced peak is present than in the deuteron case. Furthermore these reactions do not present any specific experimental problem having three charged particles and only a neutral one in the initial and final states.

References

1) B. L. Berman, L. J. Koester and J. H. Smith, Phys. Rev. **133** (1964) B117
2) E. Finckh, R. Kosiek, K. H. Lindenberger, U. Meyer-Berkhout, N. Nücker and K. Sablupmann, Phys. Lett. **7** (1963) 271
3) C. Becchi, G. E. Manuzio, L. Meneghetti and S. Vitale, Phys. Lett. **8** (1964) 322
4) J. R. Stewart, R. C. Morison and J. S. O'Connell, Phys. Rev. **138** (1965) B372
5) R. Bösch, J. Lang, R. Müller and W. Wölghi, Phys. Lett. **8** (1964) 120
6) V. N. Fetisov, A. N. Gorbunov and A. T. Karfoloniev, Nucl. Phys. **71** (1965) 305
7) N. M. O'Fallon, L. J. Koester and J. H. Smith, to be published
8) H. M. Gerstenberg and J. S. O'Connell, Phys. Rev. **144** (1966) 834
9) B. F. Gibson, Nucl. Phys. B2 (1967) 501;
   M. Verde, Helv. Phys. Acta **23** (1950) 453;
   J. C. Gunn and J. Irving, Phil. Mag. **42** (1951) 1353;
   C. Rossetti, Nuovo Cim. **14** (1959) 1171;
   V. Eichmann, Z. Phys. **175** (1963) 115;
   V. N. Fetisov, Nucl. Phys. **98** (1967) 437;
   J. M. Knight, J. S. O'Connell and F. Prats, Phys. Rev. **164** (1967) 1354;
   I. M. Barbour and A. C. Phillips, MIT-CTP 100 (1969);
   R. I. Dzhibuti, V. I. Mamasakhlyov and T. S. Macharadze, Sov. J. Nucl. Phys. **2** (1966) 40
10) N. J. Carron, Phys. Rev. **168** (1968) 1095
11) A. N. Gorbunov, Phys. Lett. **27** (1968) B436
12) H. G. Clerc, R. J. Stewart and R. C. Morison, Phys. Lett. **18** (1965) 316
13) D. S. Gemmell and G. A. Jones, Nucl.. Phys **33** (1962) 102
14) J. E. Perry and S. Bame, Phys. Rev. **99** (1955) 1368
15) B. H. Bransden, A. C. Douglas and H. H. Robertson, Phys. Mag. **2** (1957) 1211
16) R. I. Dzhibuti, N. D. Krupeninkova and V. I. Mamasakhlisov, Sov. J. Nucl. Phys. **7** (1968) 489;
   L. Crone and C. Werntz, Nucl. Phys. **A134** (1969) 161;
   J. Hufner and C. M. Shakin, Phys. Rev. **175** (1968) 1350;
   F. Beck and A. Muller-Arnke, Phys. Lett. **27B** (1968) 343
17) R. I. Dzhibuti and A. V. Tagviashvili, JETP (Sov. Phys.) **12** (1961) 1225
18) P. Picozza, C. Schaerf, R. Scrimaglio, G. Goggi, A. Piazzoli and D. Scannicchio, Nuovo Cim. **55A** (1968) 206

19) P. Picozza, C. Schaerf, R. Scrimaglio, G. Goggi, A. Piazzoli and D. Scannicchio, Nuovo Cim. Lett. **2** (1969) 445
20) C. Keck and A. V. Tollestrup, Phys. Rev. **101** (1956) 360
21) R. Ching and C. Schaerf, Phys. Rev. **141** (1966) 1320
22) I. Modena, V. Montelatici and F. Scaramuzzi, Nucl. Instr. **44** (1966) 175
23) G. P. Milburn, N. Birnbaum, W. E. Crandall and L. Scheiter, Phys. Rev. **95** (1954) 1268
24) P. Picozza, C. Schaerf, R. Scrimaglio, G. Goggi, A. Piazzoli and D. Scannichico, internal report INFN/AE-69/10 (1969)
25) N. Austern, Phys. Rev. **100** (1955) 1522
26) R. R. Wilson, Phys. Rev. **104** (1956) 218
27) M. Davier, D. Benaksas, D. Drickey and P. Lehman, Phys. Rev. **137** (1965) B119
28) S. Barshay, Phys. Lett. **17** (1965) 78
29) J. Bernstein, G. Feinberg and T. D. Lee, Phys. Rev. **139** (1965) 1650
30) S. Barshay, Phys. Rev. Lett. **17** (1966) 49
31) M. Longo, Bull. Am. Phys. Soc. **14** (1969) 598
32) D. Bachelier, M. Bernas, I. Brisand, C. Detraz, J. P. Didelez, H. Longevin-Joliot, J. K. Lee and P. Radvanji, Phys. Lett. **21** (1966) 697
33) D. F. Bartlett, C. E. Friedberg, K. Goulianos, I. S. Hammerman and D. P. Hutchinson, Phys. Lett. **23** (1969) 893